

# Peer-Reviewed Technical Communication

## Testing and Characterization of a Fixed Wing Cross-Domain Unmanned Vehicle Operating in Aerial and Underwater Environments

Warren Weisler<sup>✉</sup>, William Stewart, Mark B. Anderson, Kara J. Peters, Ashok Gopalarathnam, and Matthew Bryant

**Abstract**—This paper presents test results and performance characterization of the first fixed-wing unmanned vehicle capable of full cross-domain operation in both the aerial and underwater environments with repeated transition and low-energy loitering capabilities. This vehicle concept combines the speed and range of an aircraft with the persistence, diving capabilities, and stealth of a submersible. The paper describes the proof-of-concept vehicle including its concept of operations, the approaches employed to achieve the required functions, and the main components and subsystems. Key subsystems include a passively flooding and draining wing, a single motor and propeller combination for propulsion in both domains, and aerodynamic–hydrodynamic control surfaces. Experiments to quantify the vehicle performance, control responses, and energy consumption in underwater, surface, and flight operation are presented and analyzed. Results of several full-cycle tests are presented to characterize and illustrate each stage of operation including surface locomotion, underwater locomotion, water egress, flight, and water ingress. In total, the proof-of-concept vehicle demonstrated 12 full-cycle cross-domain missions including both manually controlled and autonomous operation.

**Index Terms**—Flying submarine, submersible aircraft, unmanned aerial-aquatic vehicle, unmanned aerial vehicle, unmanned underwater vehicle.

### I. INTRODUCTION

THE use of unmanned vehicles, including unmanned aerial vehicles (UAVs) and unmanned underwater vehicles (UUVs), has expanded greatly in recent years [1], motivated by myriad commercial and military applications. While developments have advanced the capabilities of both aerial and underwater vehicle classes, a single vehicle capable of performing in both the aerial and underwater domains has remained elusive. There has been significant interest in developing a cross-domain vehicle capable of operating seamlessly both underwater and in the air [1]–[6]. However, no previous vehicle has offered a fully functional design capable of repeated transitions between domains, low-energy loitering, and useful levels of endurance. Such a cross-domain vehicle concept would merge the benefits of operating in each of these domains, combining the persistence of a surface vehicle, the diving, underwater maneuvering, and stealth capabilities of an underwater vehicle, and the speed and range of an airborne vehicle. The cross-domain concept of operations thus greatly increases the range of sensing modalities, communication methods, and mission scenarios available to the vehicle.

Manuscript received February 28, 2017; accepted August 17, 2017. Date of publication September 18, 2017; date of current version October 11, 2018. This work was supported by SSC Pacific under Contract N66001-14-C-4008. (Corresponding author: Warren Weisler.)

**Associate Editor:** K. Von Ellenrieder.

W. Weisler, W. Stewart, K. J. Peters, A. Gopalarathnam, and M. Bryant are with the Department of Mechanical and Aerospace Engineering, North Carolina State University, Raleigh, NC 27695 USA (e-mail: [waweisle@ncsu.edu](mailto:waweisle@ncsu.edu)).

M. B. Anderson is with the Teledyne Scientific and Imaging, Durham, NC 27713 USA.

Digital Object Identifier 10.1109/JOE.2017.2742798

The existing literature considers three main subsets of UAVs with some level of water functionality: seaplane UAVs, submarine-launched UAVs, and submersible UAVs [3]. Seaplane UAVs operate and function on the water surface and in the air. These vehicles are already being tested and fielded including research vehicles such as the ACAT [7] and the Flying Fish [8], [9] as well as commercial designs such as the RQ-15 Neptune [10], Sea Scout [11], and Gull series aircraft [12]. Submarine-launched UAVs are deployed from a submerged submarine via a waterproof housing or canister that encloses the vehicle until it reaches the surface. Once launched, these vehicles perform their flight missions and are then either retrieved from the surface or discarded. This subset includes the Sea Sentry, Blackwing, and XFC UAS [13]–[15]. Within the class of submersible UAVs, several commercially available multirotor UAVs have been designed with waterproof electronics [16]–[18], and are thus capable of surviving submergence. However, none of these vehicles is designed for true underwater operation including locomotion, maneuverability, and the ability to transition between domains.

Recently, Maia *et al.* demonstrated an octocopter capable of transitioning between submerged locomotion and flight using rotary-wing lift for both flight and depth management underwater [5]. In addition, Drews *et al.* modeled and simulated a multirotor-style cross-domain vehicle, but did not construct a prototype. As in purely aerial vehicles, such rotary-wing craft benefit from high maneuverability and hover capability at the expense of a fixed-wing aircraft's endurance, range, and speed capabilities. Other researchers have turned to biology for inspiration in developing submersible UAVs. Lock *et al.* reviewed methods used by natural and robotic systems for multimodal locomotion [19], while the gannet and other diving waterfowl have also been extensively studied [4], [20]–[23]. Siddall *et al.* developed a miniature proof-of-concept water jet for launching a vehicle through the water–air interface [6]. In another paper, Siddall *et al.* studied the plunge dive behavior of a gannet-inspired morphing-wing vehicle [24]. Vehicles have also been developed to demonstrate the transition and survivability of the air-to-water transition such as Flimmer [25] and Test Sub [26]. While all of these previous studies show promise, they have yet to perform repeated bidirectional transitions with the endurance and loitering capabilities of the platform presented here.

In this paper, we present the test results and performance characterization of a fixed-wing cross-domain vehicle developed during 2014–2016 by North Carolina State University and Teledyne Scientific and Imaging. To date, efforts under this project have investigated the conceptual design of several possible vehicle architectures and demonstrated an initial proof of concept of the selected architecture [27]. Analytic and experimental efforts have addressed the dynamic modeling of passively draining vehicle compartments [28] and the design of a compact active buoyancy control engine [29]. This paper reports on untethered dynamic and energetic characterizations of the cross-domain

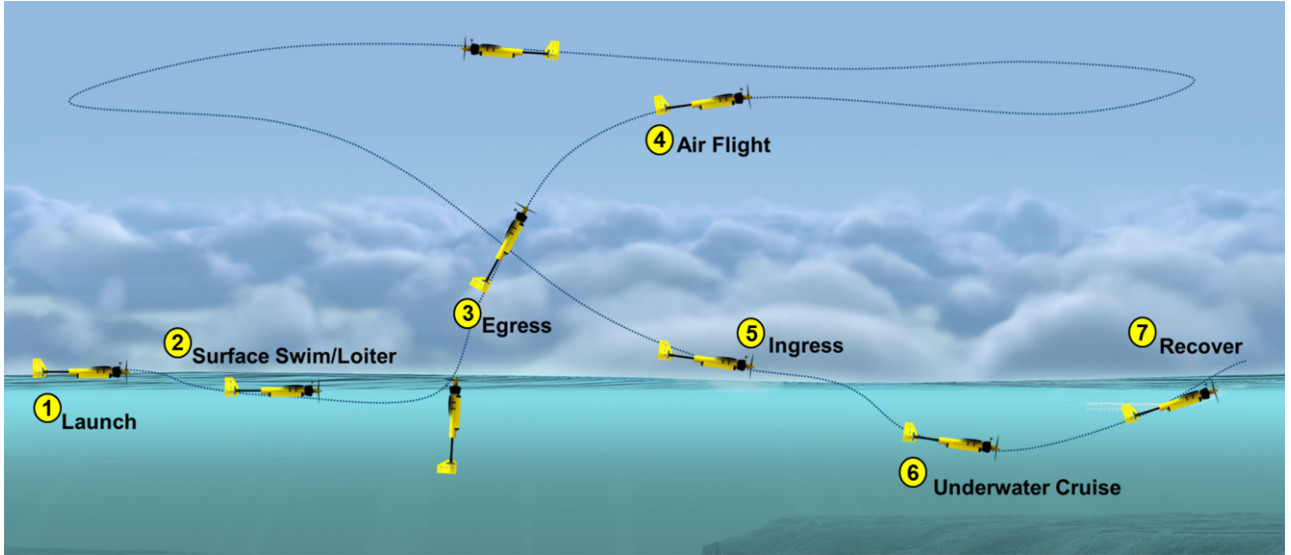


Fig. 1. Concept of operation for vehicle. (1) A full mission cycle begins by releasing the vehicle on the water surface. (2) The vehicle then cruises to its takeoff location where it stops its forward propulsion and passively loiters nose up due to its buoyancy distribution. (3) When the vehicle is in its nose-up pitch, it initiates an egress from the water, (4) followed by a vertical climb to a set altitude and transitions to forward flight. At this point the vehicle flies to its ingress location as a standard fixed-wing aircraft. (5) When the ingress location is reached, the vehicle performs a conventional fixed-wing landing, flaring just above the surface and belly landing. Then, using the motor for forward propulsion, the vehicle dives using downwards lift from its wings to overcome the small positive buoyancy of the vehicle. (6) Once below the surface, the vehicle cruises to its target. The vehicle can then either actively maneuver to the surface or passively float back up. (7) Once on the surface, the vehicle can either be recovered or can takeoff again and repeat the cycle.

vehicle operating in aerial flight, underwater locomotion, surface loiter/cruise, and transitions between domains. The data presented serve to not only validate the vehicle concept, but also illuminates design and operation issues in creating cross-domain vehicles. The remainder of the paper is organized as follows: Section II discusses the fundamental concept of operations under consideration. Section III describes the configuration of the developed and tested vehicle. In Section IV, the performance capabilities of the vehicle in the domains of interest are detailed. Section V provides the conclusions of the paper and its findings.

## II. HYBRID AERIAL AND UNDERWATER CONCEPT OF OPERATIONS

We consider a vehicle CONcept of OPerationS (CONOPS) that combines the capabilities of a fixed-wing UAV and a UUV to create a design that can operate freely across the air and water domains, rapidly transitioning as needed. As illustrated in Fig. 1, this CONOPS is decomposed into the following stages: launch, surface swim/loiter, egress, air flight, ingress, underwater cruise, and vehicle recovery. This vehicle lends itself to persistent maritime operations in which the vehicle is deployed, then performs passive monitoring. If needed, it can rapidly change locations and monitor from the new location, or fly and track a target exceeding the speed of conventional UUVs. To accomplish this CONOPS, a single vehicle capable of satisfying the fundamental operating requirements in each domain is required. As the vehicle is designed to perform multiple cycles as needed, the vehicle must stay intact throughout its operation. A video of the vehicle performing a complete CONOPS cycle is located at <https://youtu.be/Aw01NnG9hu0>.

## III. PROTOTYPE VEHICLE

### A. Management of Buoyancy, Lift, and Weight

Efficient underwater operations require a vehicle to have an overall density very close to that of water to balance the static forces acting on the vehicle: buoyancy and weight. However, for efficient air flight, a lower density airframe decreases wing loading and stall speed

while increasing efficiency. To resolve these competing requirements, the vehicle's watertight compartment volume is minimized to reduce its submerged displacement. The use of a conventional wing design would have entailed a large enclosed wing, which, while being efficient in the air, would have necessitated the addition of ballast to operate in the water due to its displaced volume. A variable ballast system based on floodable and drainable volumes mitigates the decrease in flight performance by lowering the density of the vehicle during flight. A simple passive approach is implemented for this proof-of-concept vehicle. The wing volume fills with water during ingress to allow the vehicle to achieve near-neutral buoyancy underwater, but is designed to rapidly drain the water upon egress.

The CONOPS considered requires the use of elements from both rotary-wing lift and fixed-wing lift depending on the phase of operation. Rotary-wing lift is utilized for the egress phase by orienting the vehicle vertically and using a high-thrust propulsion system. This allows the vehicle to rapidly drain while exiting the water and then climb to flight altitude. Once at flight altitude, the vehicle transitions to horizontal fixed-wing flight to maximize range and endurance in the air. Thus, this egress method does not require a long stretch of smooth water as in a seaplane takeoff.

Past studies have proposed folding wings for UAV-UUV hybrid concepts [2], [6], [30] to decrease drag during underwater locomotion. However, the CONOPS considered did not necessitate high-speed underwater operations because the vehicle could rapidly change location by transitioning to the air regime. Thus, the higher underwater drag and the slower underwater locomotion of a fixed-geometry wing were regarded as an acceptable tradeoff compared to the added complexity and weight of a folding wing.

### B. Airframe Configuration

A proof-of-concept vehicle capable of executing the entire CONOPS in a single configuration was designed and fabricated in-house. The experimental vehicle is shown in detail in Fig 2. The vehicle is configured

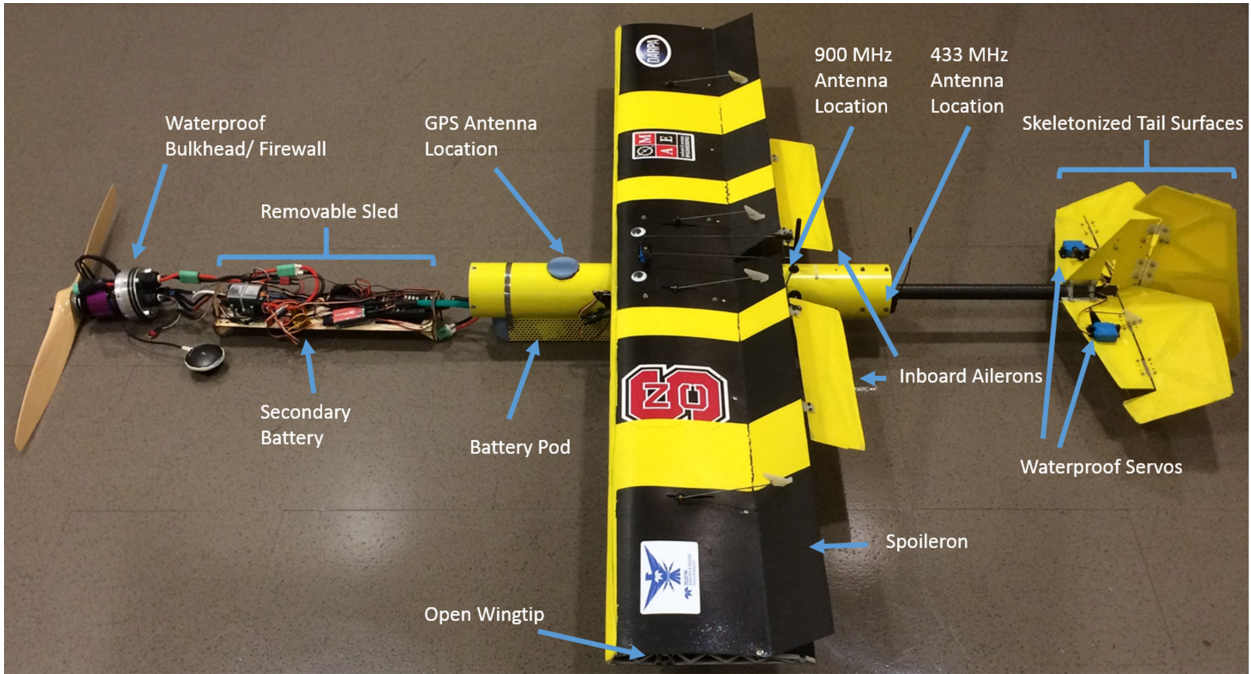


Fig. 2. Overview photograph of vehicle with sled removed and all necessary components for flight onboard.

as an aft-tail, high-wing aircraft with a wingspan of 1.5 m (59 in.), a length of 1.40 m (55 in.), and weight of 56.05 N (12.6 lbf). The airframe consists of a tubular aluminum main fuselage, composite wing, and tail. To achieve the rigidity required to survive the ingress maneuver and to facilitate rapid, passive flooding and draining, the wing uses aluminum ribs and a carbon fiber truss-spar covered in a triple-ply carbon fiber composite skin. Open wingtips allow air and water to readily exit or enter the wing during flooding and draining. The floodable space inside the wing also provides a location to place closed-cell polystyrene foam to trim the center of buoyancy (CB) and resting posture of the flooded vehicle. To permit draining during egress and also serve as roll control surfaces, the wing utilizes full-span spoilerons that can be deflected to open the trailing edge of the wing. During egress, the spoilerons are biased open to allow water to rapidly exit the wing. The spoilerons are then returned to their closed position for flight. The spoilerons are made from the aft portion of the top wing skin by integrating a continuous fiber hinge into the composite layup. Stewart *et al.* provide further details on the wing design and characterization [28]. Trailing inboard ailerons are mounted in the propeller wash, the stream of fluid accelerated by the propeller, to provide additional roll control authority to counteract propeller torque during vertical takeoff. All control surfaces are actuated by waterproof servos.

The fuselage is made from an 88.9-mm (3.5-in)-outer-diameter, 86.4-mm (3.4-in)-inner-diameter aluminum tube. Within the fuselage, a dry compartment is created by two removable aluminum bulkheads with double O-ring seals and cord grips for wire pass-through. The forward bulkhead also serves as the firewall for the motor. The wet section of the fuselage provides a protected area where waterproof payload items, antennas, and sensors can be mounted. A cruciform-shape tail with thin, flat plate surfaces is utilized to minimize buoyancy. The tail surfaces consist of skeletonized 1.59-mm (1/16-in) aluminum plate with a fiberglass covering.

The vehicle's net buoyancy and the position of its CB relative to the center of gravity (CG) are important for water operations. The CB is placed forward and above the CG to set the static equilibrium orientation of the submerged vehicle to be approximately 80°

nose-up relative to horizontal. Both the wing and battery pod positions can be adjusted longitudinally along the fuselage to tune the CG and CB locations. Since the vehicle needs to operate on the surface and underwater, managing the net buoyancy is also required. If the vehicle is negatively buoyant, it must expend energy to ascend or maintain a constant depth. However, if the vehicle is positively buoyant, energy is required to descend or maintain depth. The test vehicle is trimmed to be 0.97 N (0.22 lbf) positively buoyant. This reduces the amount of energy required to keep the vehicle submerged, but allows the vehicle to return safely to the surface if a system failure occurs.

### C. Electronics and Power Systems

Remote control, telemetry data, and GPS links are established using waterproof antennas. The water-sensitive electronics are housed in the dry compartment on a removable sled. These include the electronic speed controller (ESC), remote control receiver, telemetry radio, battery eliminator circuit (BEC), remote control switch, Pixhawk autopilot, power module (PM), cooling fan, and secondary flight battery. A schematic of the vehicle's electrical system is shown in Fig. 3 and is discussed below.

The vehicle receives command inputs from ground operators through either a remote control for manual control or a ground station computer for the autopilot. The pilot inputs are sent via remote control to the Pixhawk flight computer. For autopilot commands, Mission Planner software [31] is used to connect with the aircraft over a 900-MHz link, allowing modification of flight computer parameters and waypoints during operation, and providing telemetry data for the ground operators. The flight computer utilizes external sensors that include an external magnetometer for compass headings, a GPS for position data, a barometer for altitude, and a sonar for altitude data during landing. The Pixhawk sends the control signals to the servo motors and a throttle command to the remote control multiplexer (RC Mux). The multiplexer serves as a source selector for the ESC, allowing the operator to select either the Pixhawk-determined throttle setting or manual throttle control. For example, the system can be configured to give the pilot manual

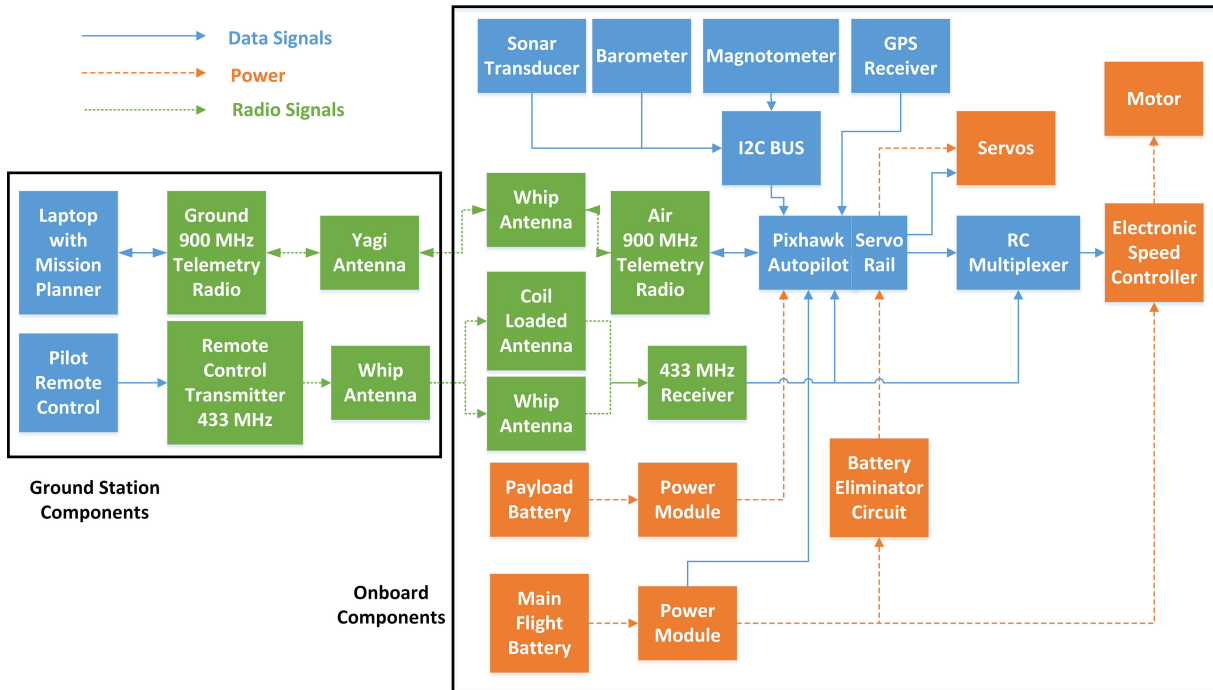


Fig. 3. Schematic of the electrical systems, showing the primary power flows, data signals, and radio signals.

throttle control but allow the flight computer to automatically stabilize the vehicle during egress. The Pixhawk also serves as the flight data recorder for the vehicle.

Electrical power is provided by two separate batteries: A main flight battery, located in an external battery pod, powers the motors and the servos, while an internal payload battery powers the flight computer and payload electronics. A PM monitors the main flight battery and passes current and voltage data to the Pixhawk. The main battery also powers a 20-A BEC and provides 5 V to the servo rail on the Pixhawk to power the servos. This acts as a redundant power source for the flight computer if the payload battery fails, utilizing the Pixhawk's built-in switching capability. The payload battery is a 850-mAh 2S LiPo (7.4 V) 25-40 C battery and is connected to an AttoPilot 180-A 50-V Voltage and Current Breakout PM, which provides the primary power to the Pixhawk.

Creating a reliable control link to the vehicle both above and below the water surface was a significant obstacle to overcome for testing. A standard remote control aircraft transmitter, a Spektrum DX9, is utilized for the control inputs, then the signals are transmitted to the aircraft using a 600-mW 433-MHz transmitter and multiantenna diversity receiver system. The signals are received with an external 433-MHz coil-loaded dipole antenna located on the tail boom and a redundant 433-MHz whip antenna in the dry compartment. The digital nature of the receivers makes testing much safer as the vehicle enters failsafe mode if signal is lost. The 900-MHz telemetry system utilizes the stock Pixhawk telemetry radios with a whip antenna on the aircraft and a Yagi antenna on the ground for improved communications with increased directionality. The 433-MHz system provides reliable control to an approximate depth of 2.4 m (8 ft) in tests in a swimming pool, while the 900-MHz link remained established up to a depth of about 0.3 m (1 ft). The ground station control setup is shown in Fig. 4.

The flight computer provides four main modes of control: full manual, fly-by-wire, autonomous with manual throttle, and full autonomous. The manual mode allows the pilot to operate the vehicle, while the autopilot records flight and water performance data. The fly-by-wire mode allows the pilot to command changes from a wings-level,

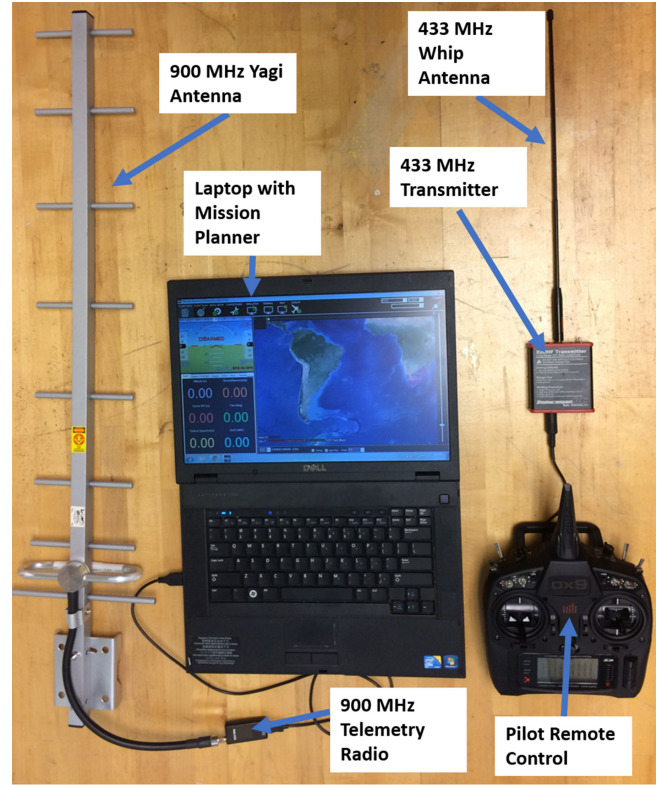


Fig. 4. Overview photograph of ground station equipment.

steady track cruising condition in both air and water operation. This enables underwater cruises even if the pilot is unable to see the vehicle. In the autopilot with throttle pass-through mode, the autopilot operates the vehicle to maintain vehicle orientation and GPS navigation while allowing the pilot manual throttle control. In full autonomous

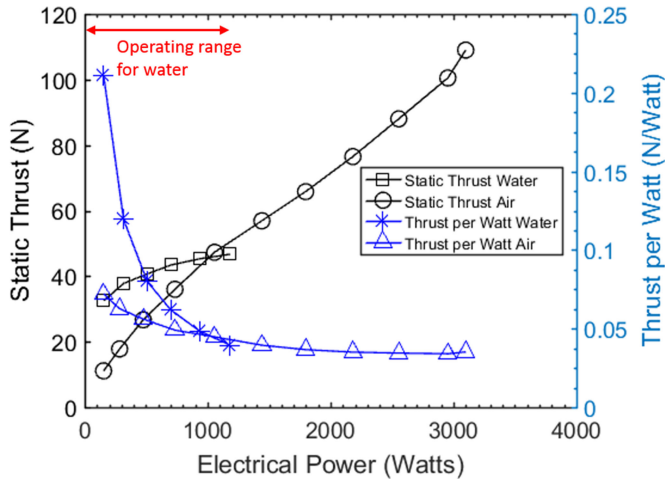


Fig. 5. Static thrust and thrust per unit power in water and air as a function of electrical power.

mode, the flight computer is responsible for all aspects of operation and navigation.

#### D. Propulsion

The vehicle is propelled using a Hacker A60 brushless motor paired with a 63.5-cm (25 in)-diameter propeller with a 25.4-cm (10-in) pitch. The motor speed is controlled by a 130-A Castle Creations ESC using a 3800-mAh 8S LiPo (29.6 V) 55C battery. This system is capable of both high-RPM air propulsion as well as low-RPM underwater propulsion while remaining within the current limits of the ESC. In static thrust testing, this combination produced 109 N (24.5 lbf) at full throttle in the air to yield a vehicle thrust to weight ratio of 1.9 and up to 46 N (10.3 lbf) thrust in the water.

Fig. 5 shows the results of the static testing in water and air. This figure shows that the same motor and propeller combination can be used in water and air, but with limited operating ranges for water. The maximum water thrust shown was for a throttle setting of only 10.5% due to ESC temperature limits with the increased load of water operation. To facilitate cooling of the ESC, a small fan circulates air in the dry compartment, and thermal pads between the ESC and the aluminum fuselage wall provide a heat conduction path. Fig. 5 shows that at power levels below 1000 W, the thrust per unit power is greater in water than air.

## IV. VEHICLE CHARACTERIZATION RESULTS AND DISCUSSION

The vehicle was field tested in five operating regimes: surface cruise, underwater cruise, egress, flight, and ingress. During testing, the vehicle's performance characteristics were recorded by the Pixhawk in conjunction with on board and ground cameras. The water performance testing was conducted in the diving well of the University pool, while full-cycle flight and water tests were performed at a University-owned lake and flight facility at Perkins Field in Bahama, NC, USA (see Fig. 6). The following sections discuss the test results of each operating regime.

#### A. Surface Operations

The range and endurance of the vehicle operating on the surface was experimentally quantified. The vehicle was trimmed with the control surfaces to a straight and level surface cruise, defined as a linear track

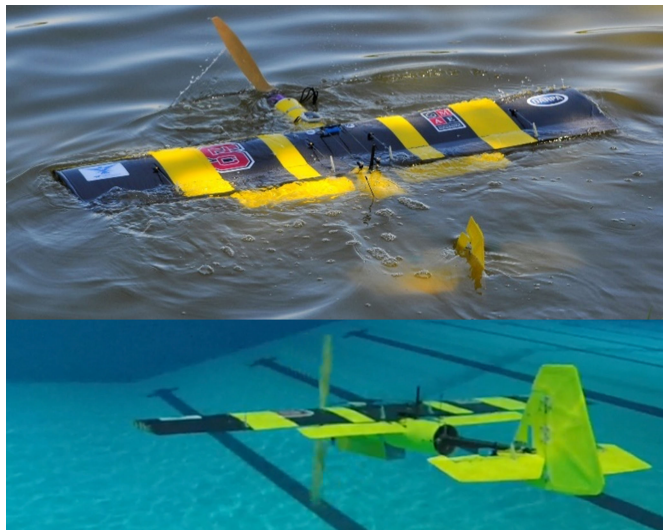


Fig. 6. (Top) Photograph of surface cruise. (Bottom) Photograph of underwater cruise.

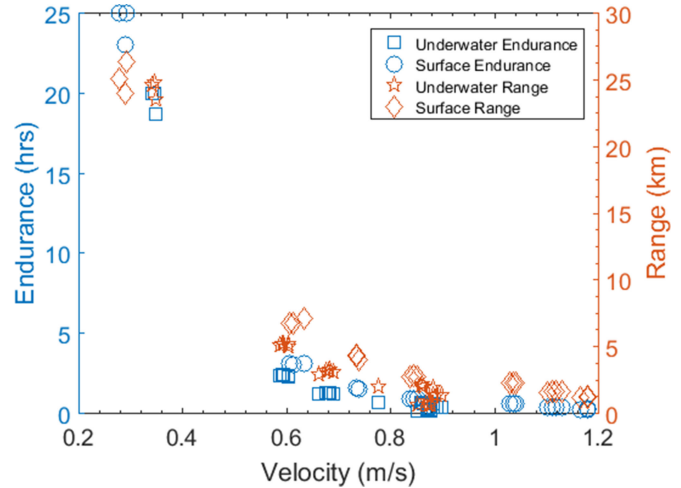


Fig. 7. Underwater and surface endurance and range as functions of velocity. The clusters of points represent discrete throttle settings in 1.5% increments from 1.5%–10.5% left to right with three trials performed for each setting.

that maintained sufficient pitch-up attitude such that displaced water did not flow over the top of the wing (see Fig. 6). For each run, the average locomotion speed and power usage were measured, and the resulting vehicle range and endurance capabilities were calculated based on the energy capacity of the battery. Fig. 7 shows that the surface range and endurance of the vehicle in water are maximized at minimum speeds. The efficiency of the vehicle is further characterized by examining the variation in velocity with electrical power for each speed (see Fig. 8). Fig. 8 shows that the vehicle is most efficient at transducing applied motor power to locomotion velocity at low power settings. Over the range tested, the velocity monotonically increases with power while the velocity per unit power monotonically decreases. These results are counter to those expected for an aircraft in flight, where operating at slow speeds, near the stall condition, results in high drag and poor efficiency. This difference occurs because a cruising aircraft must generate lift, and corresponding induced drag, to sustain flight, while a near-neutrally buoyant vehicle in water does not require significant lift and induced drag production.

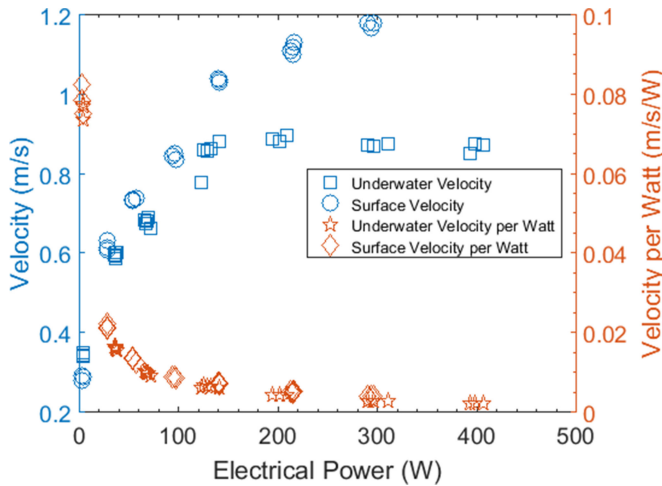


Fig. 8. Underwater and surface velocity as functions of electrical power and velocity per unit power as a function of electrical power. The clusters of points represent discrete throttle settings in 1.5% increments from 1.5%–10.5% left to right.

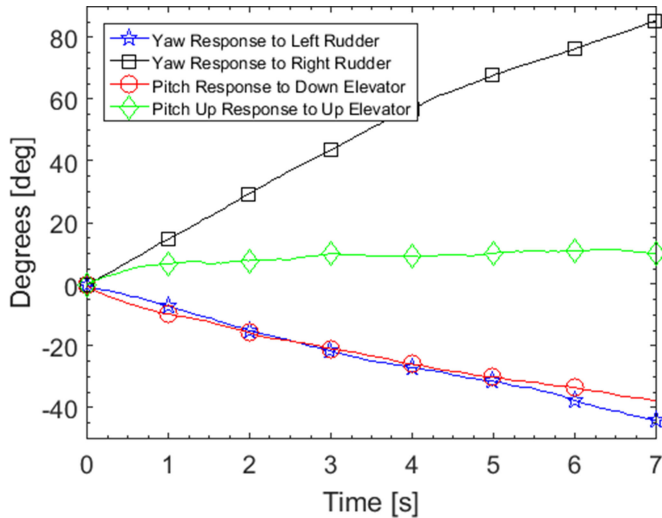


Fig. 9. Yaw response to full left and right rudder deflection and pitch response to full up and down elevator deflection during surface locomotion at 0.74 m/s initial speed. Positive degree values correspond to right yaw and pitch up. Time = 0 s corresponds to the start of full control input.

The vehicle's ability to maneuver on the surface was characterized next. To describe the motion of the vehicle, an aircraft coordinate system is defined with the  $x$ -axis pointing towards the front of the vehicle, the  $y$ -axis pointing to the right wing, and the  $z$ -axis pointing towards the bottom of the vehicle. A positive roll, pitch, or yaw response follows the right-hand rule about the axis in question. The effects of full rudder, aileron/spoileron, and elevator deflections are evaluated using the pitch and yaw data from the Pixhawk inertial measurement unit as shown in Fig. 9. As the vehicle exhibits negligible response to aileron/spoileron inputs on the surface, they are omitted from Fig. 9 for clarity.

During surface operations there is a significant difference between the left and right yaw response to rudder input. This is because only the bottom half of the clockwise-rotating propeller is in the water, pushing the nose of the vehicle to the right (i.e., creating a positive yawing moment). To compensate for this effect, 15° of left rudder is needed to achieve a linear track, thus reducing the remaining amount of left rudder range compared to right rudder range. To keep the vehicle on

the surface, 5° of up elevator is required; with full down elevator input, the vehicle is able to transition from surface cruise to fully submerged underwater cruise in 4 s.

### B. Underwater Operations

The capabilities of the propulsion system with the vehicle fully submerged were evaluated in a similar method to the surface testing, except that the vehicle was trimmed with the elevator to maintain a given depth. The endurance and range as functions of velocity are shown in Fig. 7, while velocity and velocity per unit power, as functions of electrical power, are shown in Fig. 8. Fig. 7 illustrates that the vehicle has a higher range and endurance while on the surface as compared to underwater. It is also of interest to note that the vehicle reaches a maximum speed of 0.89 m/s at 7.5% throttle and actually slows at higher throttle settings even though the power consumption continues to increase. It was observed that with the throttle set to 1.5%, the ESC read 2493 RPM, however, from video analysis, the propeller was only turning approximately 63 RPM. This is due to the low-speed, high-torque operation of the motor-propeller combination in the water. Since a brushless motor is used, the timing for the phase switching is crucial for efficient operation. While the tested motor-propeller combination provides adequate propulsion underwater, the ESC grossly misinterprets the motor speed and thus its subsequent timing. This error decreases the efficiency of the motor-propeller combination in underwater operation, as the motor poles are switched faster than the motor is rotating, and is likely responsible for the observed plateau in vehicle speed and higher efficiencies at low speeds. The large gap between the two left-most point clusters in Fig. 8 indicates the strong sensitivity of speed to power consumption at low throttle settings.

The vehicle's ability to maneuver underwater was evaluated in a manner similar to the surface testing with the vehicle trimmed to maintain a given depth with a linear track. Once the vehicle reached a steady speed, the response to sustained full input of each control surface was evaluated; right and left aileron/spoileron, right and left rudder, and up and down elevator tests were performed. For clarity, the origin for each control response plot is defined as the point where the respective control surface input reaches its full value.

Fig. 10 illustrates the roll and yaw responses to left and right aileron/spoileron inputs during underwater locomotion. As is typical for vehicles with spoileron control surfaces, proverse yaw effects are exhibited in Fig. 10. For example, when the right spoileron is deflected upward to roll the right wing downward, more drag is induced on the right wing, thus causing a clockwise yaw. This behavior is observed for all of the test cases, except the initial second of the 0.89-m/s right and left aileron/spoileron cases. This is likely due to a slower response in the spoileron servos at higher vehicle speeds because of increased dynamic pressure. The motor torque contributes to the increased roll rate observed in the negative roll tests as compared to the positive roll tests. In addition, during the 0.35-m/s trials, it is observed that the vehicle's yaw is initially dominated by the drag induced by the spoilerons. However, as the vehicle rolls past approximately  $\pm 20^\circ$ , the forward location of the CB produces a yawing moment that tends to rotate the nose toward the surface. In the 0.35-m/s case, this causes the yaw rate to change direction at approximately  $t = 4$  s in both Fig. 10(a) and (b). In the 0.68- and 0.89-m/s cases, the yaw rate does not actually change direction, but this effect is still apparent as a slowing of the yaw rates. These observations point to a competing effect between the yaw stiffness and the proverse yaw of the vehicle as a function of speed. This effect occurs because the hydrodynamic forces increase with vehicle speed, while the yawing moment due to buoyancy is independent of vehicle speed.

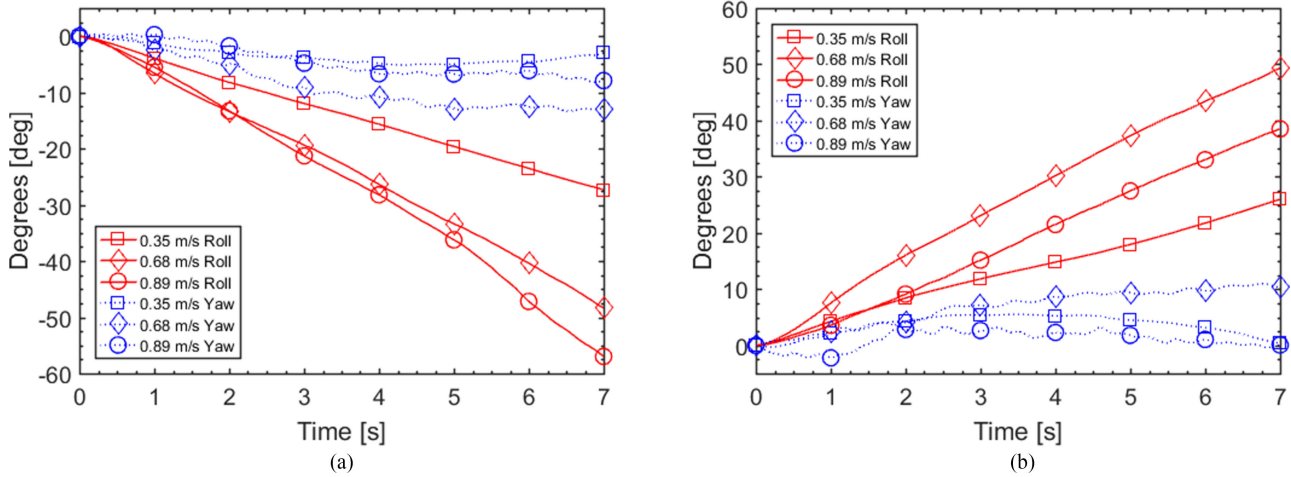


Fig. 10. (a) Roll and yaw response to left aileron and spoileron input underwater at vehicle velocities of 0.35, 0.68, and 0.89 m/s. (b) Roll and yaw response to right aileron and spoileron input underwater at vehicle velocities of 0.35, 0.68, and 0.89 m/s. Positive degree values indicate right roll and right yaw. Time = 0 s corresponds to the start of full control input.

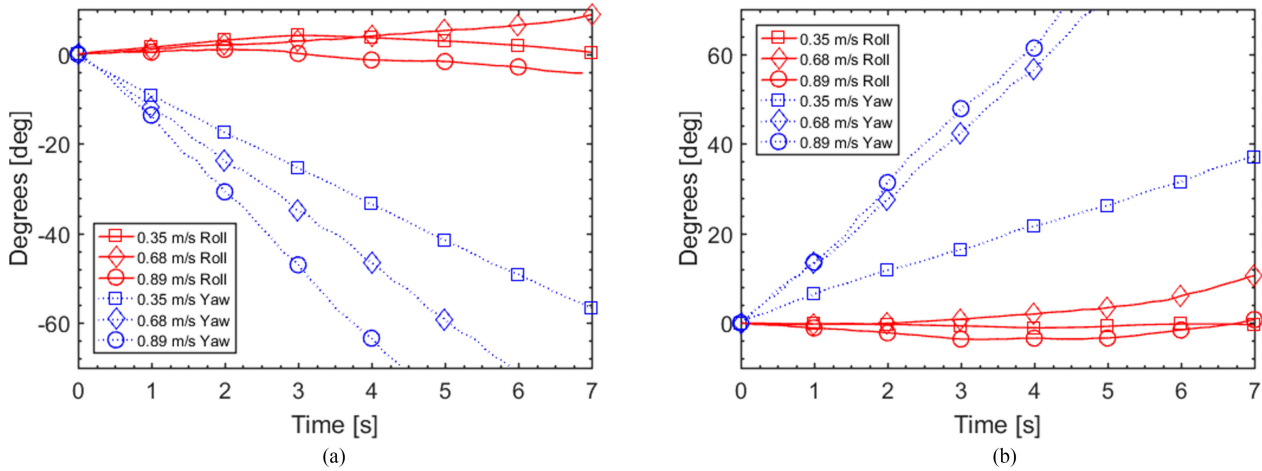


Fig. 11. (a) Roll and yaw response to left rudder input underwater at vehicle velocities of 0.35, 0.68, and 0.89 m/s. (b) Roll and yaw response to right rudder input underwater at vehicle velocities of 0.35, 0.68, and 0.89 m/s. Positive degree values indicate right roll and right yaw. Time = 0 s corresponds to the start of full control input.

Fig. 11 plots the underwater roll and yaw responses to rudder input. At the top speed of 0.89 m/s, the yaw rates in response to left and right rudder input are nearly identical in magnitude. However, the yaw rates for the other test speeds show much larger differences between left and right rudder inputs. These are more consistent with the results from the surface testing and are likely due to differences in travel of the rudder from left to right, as the rudder limits allow 15° more right rudder than left. In addition, when the vehicle is submerged, right rudder is needed to maintain a linear track due to the propeller slipstream impinging on the vertical tail, while on the surface, left rudder is needed due to the effect of the partially submerged propeller forcing the nose to the right. It can also be observed that the vehicle has an initial tendency to roll opposite the yawing turn. As the turn progresses, the vehicle roll tends to change to rolling with the yawing turn. This effect is caused by the vehicle slowing slightly during the turn due to the drag of the deflected surface. In a yawing turn, the wing on the outside of the turn is traveling faster through the water than the inside wing. With the elevator trimmed for the initial speed, the wing produces slight negative lift to counter the positive buoyancy of the vehicle. However, as the vehicle slows, the elevator pitching moment is reduced and allows the buoyancy moment to pitch the vehicle to a more nose-up orientation and change the angle

of attack of the wing. When this occurs, the outside wing generates positive lift, causing the direction of the roll to change.

The pitch responsiveness of the submerged vehicle to elevator input is shown in Fig. 12. The results show that the response to downward elevator is slower than upward elevator for comparative runs. This is due, in part, to the fact that at slower speeds the vehicle needs more down elevator to maintain depth (approximately 13° at 0.35 m/s compared to 10.8° at 0.89 m/s), leaving more elevator range available for pitch up than pitch down. Furthermore, the buoyancy of the vehicle fights the nose-down motion while it aids the nose-up motion. This nose-up pitching moment from the buoyancy also allows the vehicle to transition passively from underwater cruising to the egress orientation. When throttle is zeroed and controls are released at an initial depth of 1 m and initial speeds of 0.35 and 0.89 m/s, it takes the vehicle approximately 12 and 14 s, respectively, to passively return to the surface and pitch into the egress orientation.

### C. Water to Air Egress

With the basic capabilities of the vehicle to perform water operations evaluated, the egress phase of operation was characterized. The vehicle

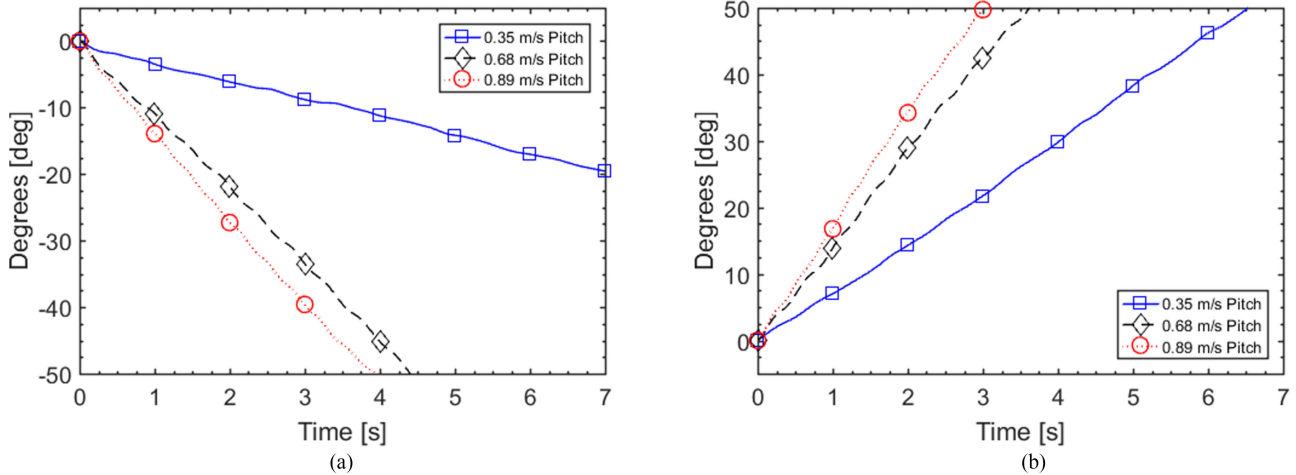


Fig. 12. (a) Pitch response to down elevator input underwater at vehicle velocities of 0.35, 0.68, and 0.89 m/s. (b) Pitch response to up elevator input underwater at vehicle velocities of 0.35, 0.68, and 0.89 m/s. Positive degree values indicate pitch up attitude. Time = 0 s corresponds to the start of full control input.

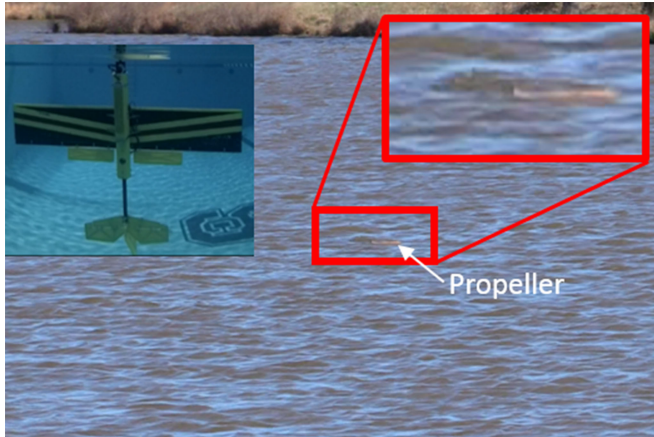


Fig. 13. Photographs of vehicle fully settled into the egress position. Note how the propeller is partially submerged in the water.

was launched from shore, cruised to the desired egress location, and was allowed to come to rest in the egress orientation shown in Fig. 13.

A typical egress maneuver consists of a five-phase sequence depicted in Fig. 15. Phase one consists of throttle start to the first appearance of the fuselage at the surface. This phase indicates that the propeller has cleared the water and thus it is safe to increase power. The second phase spans from when the fuselage breaks the surface until the wing leading edge breaches the surface. During this phase, the vehicle is being accelerated upwards and building momentum, but no significant draining occurs because the wing and wet fuselage compartments remain submerged. The third phase starts when the leading edge of the wing breaks the surface, thus starting the passive draining of the wing, and continues until the trailing edge of the wing clears the surface. During this phase, the vehicle becomes increasingly unstable in pitch, as the stabilizing effects of the wing against heave decrease as the wing exits the water. From the time when the wing starts to exit the water until the tail emerges from the water, the vehicle is also more susceptible to wind disturbances. The fourth phase lasts from when the trailing edge of the wing leaves the water until the vehicle is completely clear of the water. During this phase, the draining of the fuselage wet compartment and the tail boom occur. The fifth phase starts when the tail clears

the water and lasts until the vehicle is pitched down into horizontal flight. During this phase, the throttle is increased to full throttle to gain altitude, airspeed, and subsequent controllability.

To facilitate the passive water draining from the wing, both spoilerons are biased  $10^\circ$  open during the entire egress maneuver [Fig. 14(c)]. This allows both sides of the wing to have an open draining path during the most critical draining phases of the egress, and still allows adequate roll control authority as needed. The vehicle performance and maneuverability on egress could likely be improved by optimizing the time duration that the spoilerons are held open during egress. It is desirable for them to be open long enough to allow sufficient water draining, but also to close as soon as possible to improve controllability.

Timestamped photographs of the egress maneuvers, along with plots of the height of the propeller above water, vertical velocity, commanded throttle, current, and energy consumed as functions of time are shown in Figs. 14 and 15 for two manual egress maneuvers. Egress analysis is performed by collecting throttle, current, and energy-consumed data from the Pixhawk, whereas the height above water and vertical velocity are collected by performing photogrammetry on images from a stationary still camera (Nikon D7200) operating at six frames per second. The only modifications made to the vehicle between the two tests were minor changes to the paint scheme and an improved battery pod, thus increasing the mass of the vehicle by 91 g (0.2 lbm) from the Fig. 14 trial to the Fig. 15 trial. The egress in Fig. 14 shows that the pilot reduces throttle at  $t = 2.5$  s after judging that the vehicle had sufficient controllability. Comparing the throttle histories between the two egresses, it is apparent that the pilot frequently adjusted throttle in egress 1 (see Fig. 14), but only increased throttle incrementally in egress 2 (see Fig. 15). The time for the tail to clear the water was 1.97 and 1.67 s for egress 1 and 2, respectively, and the overall energy consumed was 1.93 and 1.96 kJ for egress 1 and 2, respectively. From these results, it was observed that egress 2 occurred in 15% less time than egress 1 while consuming 1.5% more energy.

To test the performance of the onboard autopilot in automating the water egress maneuver, the flight controller was programmed to climb to an initial waypoint altitude while maintaining wings level and a  $70^\circ$  pitch orientation. For safety, the throttle was manually controlled by the pilot as an autopilot pass-through variable, while the autopilot controlled all other outputs autonomously. Fig. 16 shows a composite image of one such automated egress performed in high wind conditions.

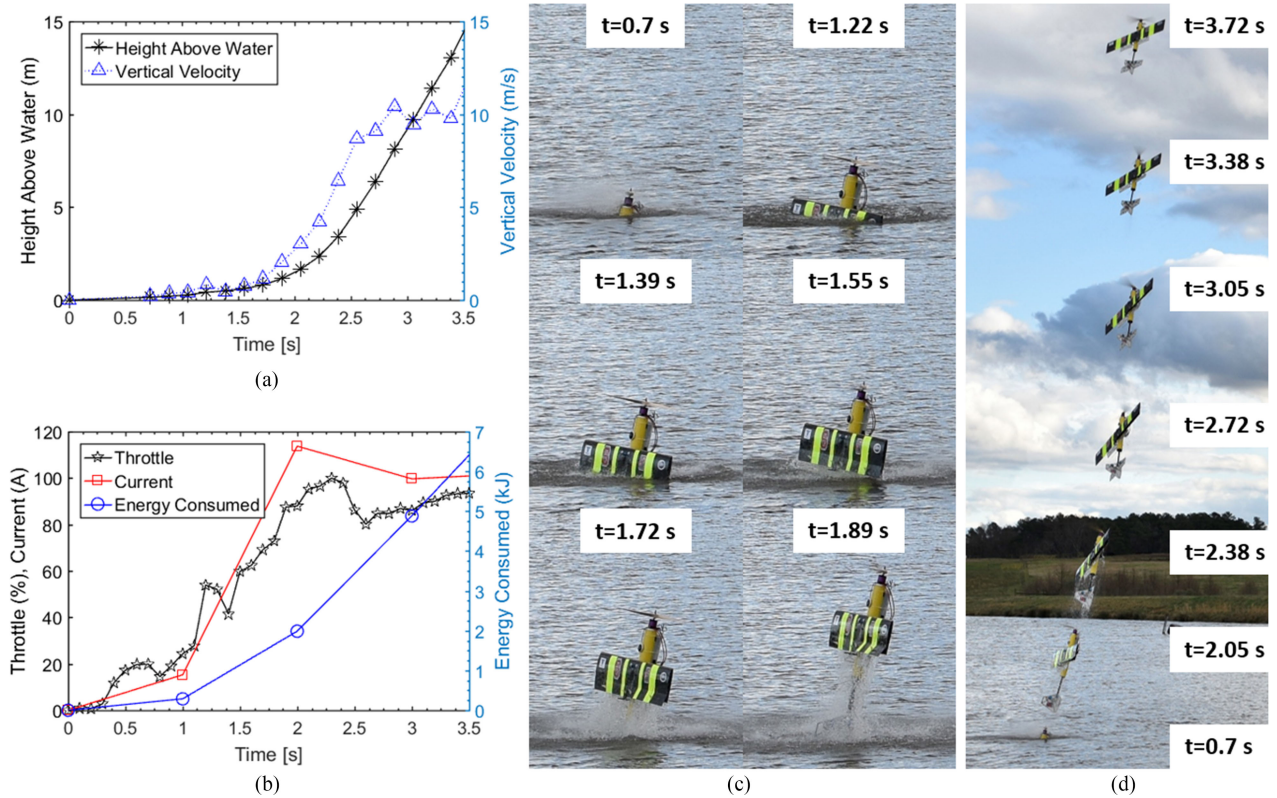


Fig. 14. Egress 1 characterization. (a) Plot of height above water and vertical velocity as functions of time. (b) Plot of commanded throttle, current, and total consumed energy as functions of time. (c) Timestamped photograph sequence, with  $t = 0$  s defined when the throttle was engaged. (d) Composite image illustrating egress trajectory overview.

When the wings exit the water, the wind starts to pitch the vehicle into an inverted orientation. The autopilot counters by rolling to wings level and climbing as the vehicle travels downwind. This test illustrates the vehicle's susceptibility to pitch disturbances due to wind during egress, but that the autopilot can correct the orientation and maintain stability. The Pixhawk autopilot is used due to the open source code, which allows customization of flight and operating parameters. One of the limitations of the Pixhawk autopilot is that if the pitch exceeds 90°, the flight computer accepts the reciprocal heading and rolls the aircraft, instead of pitching back through vertical to maintain the initial heading.

Fig. 17 compares the water draining from the flooded portions of the vehicle during egresses occurring at different rates. While both images show the vehicle at a similar altitude, the egress on the left occurred 0.4 s faster. Substantially more water draining is visible for the faster egress, indicating that significantly more water is entrained in the vehicle as it climbs out of the water. This observation suggests that there may be an optimum matching between the vehicle water draining rate and the vertical rate of climb during egress to minimize the mass of entrained water. However, in windy conditions, performing a rapid egress can reduce the pitch angle deviation induced by the wind impinging upon the wing planform while the tail is still submerged. The substantial water draining from the wing observed in Fig. 16 indicates the rapid nature of the egress, which was necessary to successfully complete the maneuver in the test wind conditions.

An onboard camera was utilized to film the flight shown in the left photograph of Fig. 17 and captured the view in Fig. 18. Even with the rapid egress, after 2.8 s the wing draining is nearly complete with only small droplets shed from the wing.

#### D. Flight Operations and Air to Water Ingress

Experiments during the flight operations were conducted to evaluate cruise flight energy consumption, response to control inputs, and ingress behavior. Flight data logging was performed for three consecutive manual test flights. After egress the pilot trimmed the vehicle to the desired cruise speed and then began conducting the flight test maneuvers in an oval shape pattern. For each subsequent run the trimmed speed of the vehicle was reduced. The average ground speed was used since the vehicle flew circuits and stayed in the same area, thus averaging out effects of winds aloft. The flight duration is considered from the time the egress maneuver commences until the vehicle lands in the water. The distance traveled per energy consumed is calculated using the current and position data from the Pixhawk flight computer. Using this distance per energy value and the rated capacity of the 3.8-Ah, 29.6-V battery, the range and endurance for the vehicle at that average velocity are calculated. The results are summarized in Table I.

With the vehicle trimmed, the response of the vehicle to full pilot control inputs was evaluated, as shown in Fig. 19. During initial control response testing, it was observed that the use of full rudder in the air induced potentially dangerous spins of the vehicle. As a result, the rudder inputs were greatly reduced from full rudder deflection limits at the pilot's discretion. To maintain directional control in the water and during egress, a much larger rudder is required compared to a vehicle designed only for air cruise. This is due to the requirement to counteract the yawing torque of the partially submerged propeller during surface operation, and to provide sufficient yaw authority during the low airspeed portion of egress. Therefore, it is not unexpected that full rudder deflection induces excessive sideslip angle for the vehicle in the air domain. From Fig. 19, it can be observed that the vehicle

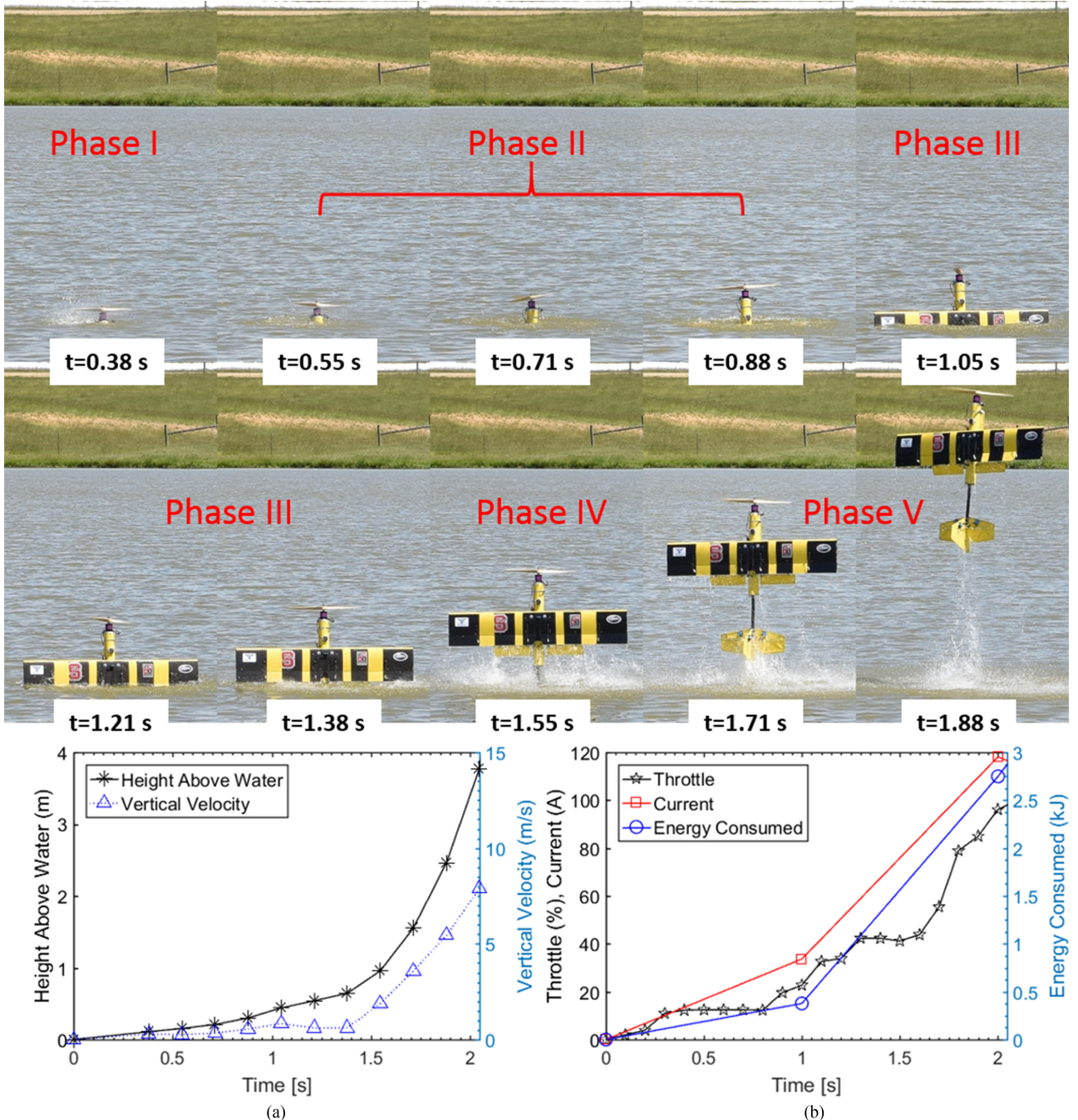


Fig. 15. Egress 2 characterization. (Top) Timestamped photograph sequence, with  $t = 0$  s defined when the throttle was engaged. (a) Vertical velocity and height above water as functions of time. Note the local peak in velocity near  $t = 1$  s, as the vehicle begins to lift the wing still filled with water above the surface, initiating the wing draining, but slowing the vertical progress. (b) Commanded throttle, current, and total consumed energy as functions of time for the egress. Note the correlation between the phases of egress and the throttle settings.

exhibits similar responses for both directions of the control surfaces at a typical flight speed. The faster negative yaw rate is consistent with the larger left rudder range than right rudder range on the vehicle.

To reenter the water, the vehicle performs the ingress maneuver, which begins with a slow approach similar to that of a conventional aircraft. Once the vehicle nears the water, it is pitched slightly up in a flare maneuver to further decrease both airspeed and sink rate. Due to the pitched-up orientation, the tail makes contact with the water first. After this, the vehicle nosed into the water and rapidly decelerates

due to the increased drag. A timestamped photograph sequence of a landing maneuver is shown in Fig. 20. The difference in pitch due to the flare maneuver can be seen between  $t = 0.17$  s and  $t = 0.33$  s. There is a balance between dissipating as much airspeed as possible in the landing flare and risking a stall causing the aircraft to enter the water in an unintended orientation. The ingress shown used only a very slight flare to enter the water in a well-controlled orientation. Of 12 ingress maneuvers performed with the vehicle, the average g-loading was 8.4 g with a standard deviation of 2.4 g and a maximum of 11.7 g.



Fig. 16. Flight controller maintaining stability with throttle pass-through with winds of 6.3 m/s gusting 9.4 m/s.

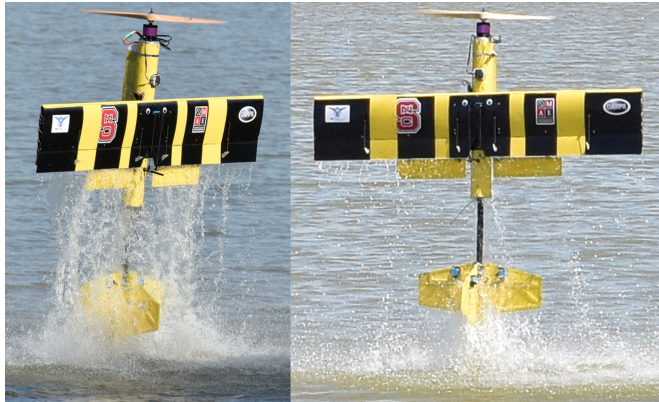


Fig. 17. Visual comparison of amount of entrained water draining for different egress speeds. (Left) Photograph of egress with 1.3-s duration to reach shown altitude. (Right) Photograph of slower egress with 1.7-s duration to reach shown altitude. Note that in the slower egress the water has nearly completely drained, whereas significant draining is still occurring for the faster egress.



Fig. 18. View from onboard camera showing nearly complete water draining 2.8 s after initiating egress maneuver. Note that spoileron is still held in the open egress position to ensure water draining. The control surface visible on the right is the leading edge of the elevator.

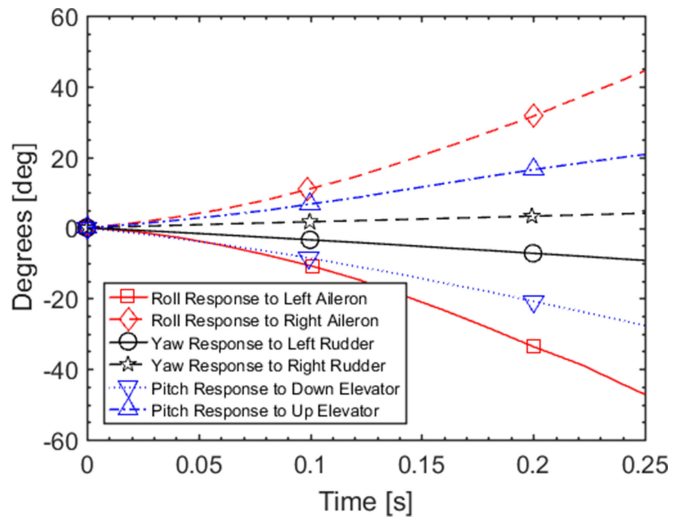


Fig. 19. Vehicle response to control inputs in flight. All control surface deflections are full except for the left and right rudder which are limited to 14° left and 11° right per safety pilot discretion. The control responses above were logged during typical vehicle cruise of approximately 19.6-m/s.

In cases where the ingress was poorly controlled, yielding of the flat-plate aluminum and fiberglass tail surfaces occurred, suggesting that these surfaces should be stiffened or changed to a floodable hollow airfoil like the wing to improve reliability in future investigations. After the ingress, the vehicle cruises back to shore for data download.

#### E. Discussion of Air and Water Handling Characteristics

The aerial and underwater characterizations of the vehicle allow comparisons between the responses to control surface deflections in the two operational domains. Table II compares the air and water control responses for experiments with similar dynamic pressures of 248 Pa in air (corresponding to 19.6-m/s speed from Fig. 19) and 231 Pa in water (corresponding to the 0.68-m/s speed cases from Figs. 10–12). The response rates are calculated as the average angular displacement per time for each response test case. Then the response per distance traveled is calculated using the response time history and the apparent vehicle track. In general, it can be observed that the vehicle response rates are faster in air than in water, as indicated by the ratio of response rates all being greater than unity. However, the vehicle exhibits better spatial maneuverability in water than in air, as indicated by values less than unity for all the ratios of response per distance traveled. The most similar tracking occurs for the roll control inputs where the air response per distance is reduced by only 7% and 14% compared to the water case for negative and positive inputs, respectively. The results from the rudder input tests indicate that even with the significant reduction in air rudder deflection as compared to water rudder deflection, the responses still follow the trend of faster response rates but lower spatial maneuverability in air as compared to water. For pitch changes, the response per distance traveled is approximately 3 and 5 times greater in water for negative and positive inputs, respectively. These results indicate that not only are the vehicle control responses domain-dependent, but that the choice of operating domain affects each control response differently. Additionally, the enhanced spatial maneuverability in the water domain could be advantageous for applications requiring close inspection of underwater structures.

TABLE I  
MASS, FLIGHT DURATION, AVERAGE VELOCITY, DISTANCE TRAVELED, DISTANCE PER kJ, ESTIMATED RANGE, AND ESTIMATED ENDURANCE FOR THREE FLIGHTS OF THE VEHICLE

Flight test number	Mass (kg)	Flight duration (sec)	Average velocity (m/s)	Distance traveled (km)	Distance per kJ (m/kJ)	Estimated range (km)	Estimated endurance (min)
1	5.81	371	22	8.16	31.5	12.8	9.5
2	5.81	446	19	8.47	38.8	15.7	13.7
3	6.06	365	18	6.57	37.9	15.3	14.2

Note the increased mass for flight 3 was due to the addition of an onboard camera.

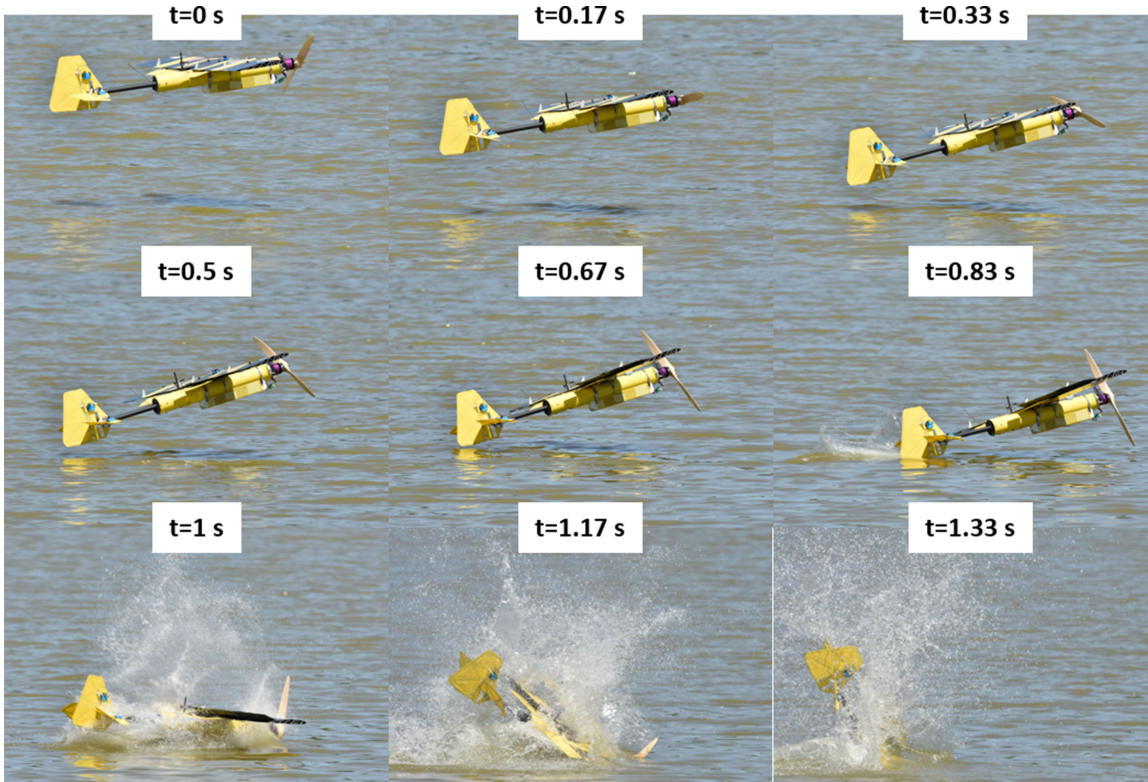


Fig. 20. Photograph sequence of landing flare and ingress at approximately 13 m/s ground speed. The vehicle experienced a peak deceleration of 5.1 g during this ingress maneuver.

TABLE II  
COMPARISON OF VEHICLE CONTROL RESPONSES IN AERIAL AND UNDERWATER OPERATION AT SIMILAR DYNAMIC PRESSURES OF 248 Pa AT 19.6 m/s IN AIR AND 231 Pa AT 0.68 m/s IN WATER.

		Air			Water			Air/Water		
Control input	Reported control response	Control surface deflection (°)	Response rate (°/s)	Response per distance (°/m)	Control surface deflection (°)	Response rate (°/s)	Response per distance (°/m)	Ratio of control surface deflections	Ratio of response rates (-)	Ratio of response per distance (-)
Negative aileron/spoileron	Roll	25/45	-184.6	-9.4	25/45	-6.9	-10.2	1	26.7	0.93
Positive aileron/spoileron	Roll	23/45	174.0	8.9	23/45	7.1	10.4	1	24.7	0.86
Negative rudder	Yaw	14	-36.9	-1.9	31	-11.8	-17.4	0.45	3.1	0.11
Positive rudder	Yaw	11	16.4	0.8	46	14.6	21.5	0.23	1.1	0.04
Positive elevator	Pitch	31	83.1	4.2	31	13.8	20.3	1	6.0	0.21
Negative elevator	Pitch	36	-109.4	-5.6	36	-11.3	-16.7	1	9.6	0.33

TABLE III  
REPRESENTATIVE ENERGY CONSUMPTION AND AVAILABILITY FOR KEY PHASES OF OPERATION

Egress	1.6 kJ
Vertical climb to 80 m	19.0 kJ
Air cruise at 19 m/s	38.8 m/kJ
Surface cruise at 0.6 m/s	21.4 m/kJ
Underwater cruise at 0.6 m/s	16.3 m/kJ
Available battery energy	404.9 kJ

To determine the mission profile capabilities of the vehicle, an energy budget can be developed using the energy consumption results presented in Table III. This enables the prediction of mission cycles that will not exceed the available energy from the battery. For example, the results show that a possible mission profile includes three egress and climb maneuvers, 9 km of air cruise, 1 km of surface cruise, and 1 km of underwater cruise. The values listed for the water cruise phases are based on a speed of 0.6 m/s, but could be increased by cruising at a slower speed.

## V. CONCLUSION

This paper has presented the testing and characterization of a proof-of-concept fixed-wing, cross-domain unmanned vehicle capable of repeatedly transitioning between underwater, surface, and flight operations. The vehicle manages buoyancy passively by using floodable compartments in both the fuselage and wing, allowing nearly neutral buoyancy in the water while minimizing the vehicle weight for flight. The floodable wing uses integrated spoilerons and open wing tips to enable rapid water draining, while inboard ailerons provide roll control during vertical egress. Only a small dry electronics compartment is included in the fuselage, and with proper potting of the electronics in the future, the dry compartment could be eliminated. The relationships between the CB and the CG and their effects on vehicle performance in both domains need careful consideration in the design of such a vehicle. For air operation, it is critical that the CG is forward of the neutral point for stability, while for water operation, placing the CB forward of the CG affords the vehicle a stable equilibrium orientation for vertical egress.

The energy consumption and control responses of the developed vehicle were characterized in surface operation, underwater cruise, egress, air flight, and ingress experiments. During the vehicle testing and characterization process and 12 full cross-domain mission cycles, it was demonstrated that the same propulsion system could be used in both air and water, with the vehicle achieving functional operation in all domains. Comparing the control responses between the operating domains showed that a simple scaling of control inputs was not sufficient to compensate for domain-dependent effects and that individual control scaling terms were required. Other domain-dependent settings included limiting the maximum throttle setting for water operations, biasing the spoilerons open during the egress maneuver, and limiting the rudder deflections for air operation. Importantly, these domain-dependent requirements were only software settings; no physical alterations to the vehicle were needed, enabling the vehicle to readily and repeatedly transition between air and water operation. Autonomous egress and flight were presented using an off-the-shelf open-source autopilot. Due to the low cost of the vehicle, it is a viable option for missions that require an expendable vehicle. This work has thus characterized a single fixed-wing vehicle capable of full cross-domain aerial and underwater operation, opening the door to new missions and applications for unmanned systems.

## ACKNOWLEDGMENT

The views, opinions, and/or findings expressed are those of the author(s) and should not be interpreted as representing the official views or policies of the Department of Defense or the U.S. Government.

## REFERENCES

- [1] P. L. Drews, A. A. Neto, and M. F. Campos, "Hybrid unmanned aerial underwater vehicle: Modeling and simulation," in *Proc. 2014 IEEE/RSJ Int. Conf. Intell. Robots Syst.*, Chicago, IL, USA, 2014, pp. 4637–4642.
- [2] A. Fabian, Y. Feng, E. Swartz, D. Thurmer, and R. Wang, "Hybrid aerial underwater vehicle," MIT Lincoln Laboratory, Lexington, MA, USA, 2012.
- [3] X. Yang, T. Wang, J. Liang, G. Yao, and M. Liu, "Survey on the novel hybrid aquatic-aerial amphibious aircraft: Aquatic unmanned aerial vehicle (AquaUAV)," *Prog. Aerosp. Sci.*, vol. 74, pp. 131–151, 2015.
- [4] J. Liang, X. Yang, T. Wang, G. Yao, and W. Zhao, "Design and experiment of a bionic gannet for plunge-diving," *J. Bionic Eng.*, vol. 10, no. 3, pp. 282–291, 2013.
- [5] M. M. Maia, P. Soni, and F. J. Diez-Garias, "Demonstration of an aerial and submersible vehicle capable of flight and underwater navigation with seamless air-water transition," 2015. [Online]. Available: <https://arxiv.org/abs/1507.01932>
- [6] R. Siddall and M. Kovac, "Launching the AquaMAV: bioinspired design for aerial-aquatic robotic platforms," *Bioinspiration Biomimetics*, vol. 9, no. 3, 2014, Art. no. 031001.
- [7] G. Pisanich and D. S. Morris, "Fielding an amphibious UAV: development, results, and lessons learned," in *Proc. 21st Digit. Avionics Syst. Conf.*, Washington, DC, USA, 2002, pp. C4-1–C4-9.
- [8] R. Eubank, E. Atkins, and D. Macy, "Autonomous guidance and control of the flying fish ocean surveillance platform," in *Proc. AIAA Infotech@Aerospace Conf.*, Seattle, WA, USA, 2009, pp. 2009–2021.
- [9] D. Macy, R. Eubank, and E. Atkins, "Flying fish: A persistent ocean surveillance buoy with autonomous aerial repositioning," in *Proc. 2008 AUVS Conf.*, San Diego, CA, USA, 2008, pp. 87–101.
- [10] DRS Technologies, "Neptune UAV." [Online]. Available: <https://www.unols.org/sites/default/files/Neptune%20UAV.pdf>. Accessed on: Dec. 19, 2016.
- [11] Business Wire, "Oregon Iron Works Successfully Completes First Auto-Landing Test of Unmanned Seaplane," May 2006. [Online]. Available: <http://www.oregoniron.com/news-and-announcements/oregon-iron-works-inc-successfully-completes-first-auto-landing-test-of-unmanned-seaplane/>
- [12] Warrior (Aero-Marine) Ltd, "Gull-Introduction," [Online]. Available: <http://www.warrioraero.com/GULL/>. Accessed on: Aug. 6, 2016.
- [13] Kollmorgen, "Sea Sentry Organic Submarine Launched UAV" [Online]. Available: [http://www.clermark.com/documents/sea\\_sentry.pdf](http://www.clermark.com/documents/sea_sentry.pdf). Accessed Nov. 2, 2016.
- [14] R. Sisk, "US Navy to Deploy Sub-Launched Spy Drones," Defense Tech, May 2016. [Online]. Available: <http://www.defensetech.org/2016/05/17/us-navy-to-deploy-sub-launched-spy-drones/>
- [15] D. Parry, "Navy Launches UAV from Submerged Submarine," Navy Research Lab, Dec. 2013. [Online]. Available: <http://www.nrl.navy.mil/media/news-releases/2013/navy-launches-uav-from-submerged-submarine>
- [16] QuadH2O, "Waterproof Drones—The HEXH2O and QUADH2O Professional Waterproof Drones," THE HEXH2O AND QUADH2O PROFESSIONAL WATERPROOF DRONES, [Online]. Available: <https://www.quadhw2o.com/quadhw2o/quadhw2o-ready-fly/>. Accessed on: Nov. 5, 2016.
- [17] SwellPro, "Swellpro waterproof splash drone AUTO version," Swell-Pro, [Online]. Available: <http://swellpro.com/product/splash-drone-auto-version/>. Accessed on: Oct. 10, 2016.
- [18] Tayzu Robotics, "Tayzu," Tayzu Robotics, 2016. [Online]. Available: <http://www.tayzu.com/tayzu-quadra-drone.html#second>. Accessed on: Dec. 4, 2016.
- [19] R. J. Lock, S. C. Burgess, and R. Vaidyanathan, "Multi-modal locomotion: from animal to application," *Bioinspiration Biomimetics*, vol. 9, no. 1, 2014, Art. no. 011001.
- [20] X. Yang, J. Liang, Y. Li, H. Zhang, and H. Xiao, "Modeling and analysis of variable buoyancy device imitating waterfowl plumage structure," in *Proc. 21st Int. Offshore Polar Eng. Conf.*, Maui, HI, USA, 2011, pp. 230–234.

- [21] T. M. Wang, X. B. Yang, J. H. Liang, G. C. Yao, and W. D. Zhao, "CFD based investigation on the impact acceleration when a gannet impacts with water during plunge diving," *Bioinspiration Biomimetics*, vol. 8, no. 3, 2013, Art. no. 036006.
- [22] X. Yang, T. Wang, J. Liang, G. Yao, Y. Chen, and Q. Shen, "Numerical analysis of biomimetic gannet impacting with water during plunge-diving," in *Proc. IEEE Int. Conf. Robot. Biomimetics*, Guangzhou, China, 2012, pp. 569–574.
- [23] J. Liang, G. Yao, T. M. Wang, X. Yang, W. Zhao, G. Song, and Y. Zhang, "Wing load investigation of the plunge-diving locomotion of a gannet Morus inspired submersible aircraft," *Sci. China Technol. Sci.*, vol. 57, no. 2, pp. 390–402, 2014.
- [24] R. Siddall, A. O. Ancel, and M. Kovac, "Wind and water tunnel testing of a morphing aquatic micro air vehicle," *Interface Focus*, vol. 7, 2016, Art. no. 20160085.
- [25] D. Edwards, "Flying-Swimmer (Flimmer) UAV/UUV," nd. [Online]. Available: <https://www.nrl.navy.mil/lasr/content/flying-swimmer-flimmer-uavuv>. Accessed on: Dec. 13, 2016.
- [26] T. Young, "Design and testing of an air-deployed unmanned underwater vehicle," in *Proc. 14th AIAA Aviation Technol., Integration, Oper. Conf.*, 2014. [Online]. Available: <https://doi.org/10.2514/6.2014-2721>
- [27] W. Stewart *et al.*, "Design and demonstration of a fixed wing hybrid UAV-UUV system," *J. Aerospace Sci. Technol.*, to be submitted.
- [28] W. Stewart, W. Weisler, M. Anderson, M. Bryant, and K. Peters, "Dynamic modeling of passively draining structures for aerial-aquatic unmanned vehicles," *J. Aircraft*, in review.
- [29] M. MacLeod and M. Bryant, "Dynamic modeling, analysis, and testing of a variable buoyancy system for unmanned multidomain vehicles," *IEEE J. Ocean. Eng.*, vol. 42, no. 3, pp. 511–521, Jul. 2017. p. doi: 10.1109/JOE.2016.2586802.
- [30] X. Yang *et al.*, "Computational simulation of a submersible unmanned aerial vehicle impacting with water," in *Proc. 2013 IEEE Int. Conf. Robot. Biomimetics*, 2013, pp. 1138–1143.
- [31] ArduPilot Dev Team, "Mission planner overview," [Online]. Available: <http://ardupilot.org/planner/docs/mission-planner-overview.html>. Accessed on: Dec. 4, 2016.



**Warren Weisler** received the B.M. degree in voice performance from the University of North Carolina at Chapel Hill, Chapel Hill, NC, USA, in 2009, and the B.S. degree in mechanical engineering in 2014 from North Carolina State University, Raleigh, NC, USA, where he is currently working toward the Ph.D. degree.

In 2014, he worked as a Support Equipment intern with the Naval Air Systems Command at Cherry Point, NC, USA. He is currently working as a Research Assistant in the Intelligent Structures and Systems Research Laboratory, North Carolina State University, working on novel UAV design. His research interests include vehicle design, aerodynamics, dynamics, and controls.

Mr. Weisler received the Provost Doctoral Fellowship in 2015, the Garrett Fellowship 2014, and the MAE Centennial Assistantship 2015–2019.



**William Stewart** received the B.S. degree in aerospace engineering and the M.S. degree from North Carolina (NC) State University, Raleigh, NC, USA, in 2011 and 2014, respectively and is currently working toward the Ph.D. degree.

From 2010 through 2014, he was a leader of the NC State University Aerial Robotics Team. In 2013, he worked on the Dream Chaser spacecraft structures team at the Sierra Nevada Corporation developing a structural acceptance testing harness. From 2014 to 2016, he has worked as a Research Assistant on the Eagle Ray project for the Smart Composites Lab. His research interests include aerodynamics, dynamics, vehicle design, and nondestructive testing.

Mr. Stewart is a two-time AUVSI student UAS competition champion, 2010 and 2014. He is Fellow of the American Society For Nondestructive Testing.



**Mark B. Anderson** received the B.S. degree in applied mathematics from the University of Wisconsin-Stout, Menomonie, WI, USA.

He is the Director of the Information Sciences Division and Chief UAS Pilot for Teledyne Scientific & Imaging, Durham, NC, USA. In this capacity, he leads an organization that is focused on both applied research and advanced technology development with more than 30 research staff, performing approximately \$7M of contract R&D per year for government and commercial customers. Before joining TS&I, he founded Security Force Software, a network security company that specialized in intrusion detection and vulnerability assessment software, which he sold to Hewlett-Packard. He is an experienced Program Manager and Researcher with more than 28 years of experience in all aspects of software development, autonomous systems, network security, anti-tamper, and data communications. He is an avid drone enthusiast and pilot and holds an FAA part 107 remote pilot certificate.



**Kara J. Peters** received the Ph.D. degree in aerospace engineering from the University of Michigan, Ann Arbor, MI, USA, in 1996.

Until 2000, she was a Researcher Collaborator at the Ecole Polytechnique Fédérale de Lausanne, Lausanne, Switzerland, in the Laboratory of Applied Mechanics and Reliability. In 2000, she joined the Faculty of the Department of Mechanical and Aerospace Engineering, North Carolina State University, Raleigh, NC, USA, where she conducts research on optical fiber sensors and composite structures. She

is currently serving as a Program Director at the National Science Foundation for the Mechanics of Materials and Structures Program.



**Ashok Gopalarathnam** received the B.Tech. and M.S. degrees from the Indian Institute of Technology, Madras, India, in 1989 and 1993, respectively, and the Ph.D. degree from the University of Illinois at Urbana-Champaign, Champaign, IL, USA, in 1999, all in aerospace engineering.

He has worked in aircraft aerodynamics and design at the National Aerospace Laboratories, Bangalore, India, during 1991–1994, at Scaled Composites in 1998, and as a Consultant to various companies since then. He is now a Professor of mechanical and aerospace engineering at North Carolina State University, Raleigh, NC, USA, where he leads the Applied Aerodynamics Research Group. His research interests include applied aerodynamics, including unsteady and post-stall aerodynamic prediction techniques, aerodynamic sensing, aircraft flight mechanics, and design.



**Matthew Bryant** received the B.S. degree from Bucknell University, Lewisburg, PA, USA, in 2007, and the M.S. and Ph.D. degrees from Cornell University, Ithaca, NY, USA, in 2011 and 2012, respectively, all in mechanical engineering.

He is an Assistant Professor in the Department of Mechanical and Aerospace Engineering, North Carolina State University, Raleigh, NC, USA. He has published more than 40 journal and conference papers. His research interests include the dynamics and control of smart structures and mechatronic systems with applications to novel actuation techniques, energy harvesting devices, fluid-structure interactions, and robotics in the land, air, and underwater domains.